ORGANIC CHEMISTRY FRONTIERS

RESEARCH ARTICLE

View Article Online
View Journal

Cite this: DOI: 10.1039/d6qo00249h

A modular family of chiral cavitand receptors: tuning the chiroptical response of achiral fullerene guests

Hugo Marchi Luciano, [a] Athul Santha Bhaskaran, [a] Cristian Montiel-Andreotti, [a] Eva Prat-Font, [a,b] Fiza Fariha, [a] Pere Galán-Masferrer, [a] Marcel Swart [a,c] and Agustí Lledó [*a,b]

Received 27th February 2026,
Accepted 18th May 2026

DOI: 10.1039/d6qo00249h

rsc.li/frontiers-organic

A new family of chiral self-folding cavitand receptors based on calix[5]arene has been developed. The cavitand synthesis is modular and highly convergent, relying on a late-stage amide formation step that allows facile diversification with different chiral amines and straightforward access to either enantiomer of the host. This strategy provides access to a set of structurally diverse and conformationally flexible cavitands that efficiently bind fullerene derivatives. The resulting host–guest complexes exhibit an induced electronic circular dichroism response in the spectral window of the achiral fullerene chromophore. The modular nature of the cavitand scaffold allows tuning of the chiroptical response of a given fullerene across the visible spectrum.

Introduction

Fullerenes are spherical π-conjugated molecules with notable electronic, photophysical, and structural properties that have gained significant attention in materials science[1,2] and biomedicine,[3] among other fields. However, practical access is mainly limited to C_{60} and C_{70}, and the inherent symmetry of these molecules creates substantial challenges in efficiently obtaining new derivatives for fullerene-based applications. In this context, supramolecular chemistry has recently become a promising approach to overcome the intrinsic limitations of fullerene chemistry.[4] The selective extraction of higher fullerenes using tailored synthetic hosts is a suitable strategy for accessing the least abundant carbon cages in fullerene soot.[5–13] Similarly, carefully designed synthetic hosts have been used as supramolecular "masks" that enable regioselective and/or enantioselective functionalization of fullerenes.[14–20]

Finally, encapsulation in chiral hosts offers a promising method to induce chirality in achiral fullerene chromophores,[21–26] bypassing the cumbersome and highly inefficient synthetic routes typically used to produce chiral fullerenes.[27,28] Fullerenes with intrinsic chirality—originating from dissymmetric substitution of the spherical π system—are particularly promising for integration into circularly polarized light (CPL) detecting devices.[29] For the latter objective, practical access to synthetic receptors that can be systematically modified to fine tune the electronic structure of the host–guest complexes is crucial. However, the majority of works on the topic of fullerene molecular recognition focus on a single host structure, often with limited potential for diversification. In metal–organic cages, for instance, subtle changes in the ligand structure often result in disparate cage geometries, limiting systematic study of a given host. In addition, many of the previous studies require resolution of the host racemate by preparative chiral HPLC, which is far from ideal.

Recently, our group has developed a series of flexible cavitand receptors based on calix[5]arene that are stabilized in the folded conformation by means of cooperative hydrogen bond networks.[30–33] While receptors featuring *O*-methyl groups at the narrow rim favour narrow and irregularly shaped pinched conformers, analogues with free hydroxyl groups engage in additional hydrogen bonding at the lower rim, bringing about a wider and more spherical cavity that is suitable for the binding of fullerenes. Importantly, the synthesis of these receptors rests on a late-stage amide condensation reaction that makes them amenable to facile diversification. Fukazawa, Haino and co-workers have previously demonstrated that (achiral) calix[5]arene-based hosts are excellent receptors for fullerenes.[34–37] Herein, we report a new family of chiral spherical receptors **1a–e** based on calix[5]arene featuring aromatic panels with a range of electronic properties (Fig. 1). We then systematically study the induction of chirality onto achiral full-

[a]*Institut de Química Computacional i Catàlisi (IQCC), Universitat de Girona, Maria Aurèlia Capmany 69, 17003 Girona, Spain. E-mail: agusti.lledo@udg.edu*
[b]*Institute of Chemical Research of Catalonia (ICIQ), The Barcelona Institute of Science and Technology, Av. Països Catalans 16, 43007 Tarragona, Spain*
[c]*ICREA, Pg. Lluís Companys 23, 08010 Barcelona, Spain*

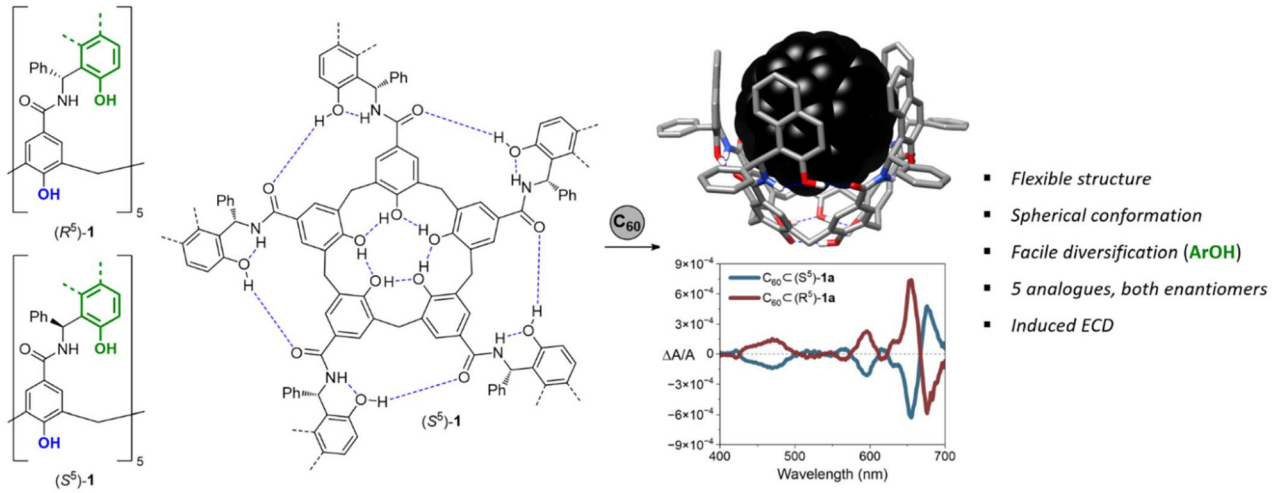

Fig. 1 Schematic structures of the new family of tunable chiral self-folding cavitands for fullerene binding and desymmetrization, and molecular model of $C_{60}\subset(S^5)$-**1a**.

erenes upon binding by **1a–e**, and rationalize the resulting electronic circular dichroism (ECD) response using molecular dynamics (MD) simulations and TD-DFT.

Results and discussion

Host synthesis and characterization

The synthesis of cavitands **1a–e** required the preparation of enantiomerically pure chiral amine building blocks **2a–e** (Scheme 1). The parent Betti base (**2a**) was synthesized and resolved *via* classical resolution using tartaric acid, as previously described in the literature (Scheme 1A).[38,39] Enantiopure bromo-naphthalene derivative **2b** was obtained following the same strategy. However, this approach proved ineffective for the preparation of amines bearing substituted phenyl rings. Amines **2c–e** were prepared in optically pure form using Ellman's chiral sulfinamide auxiliary (Scheme 1B). Diastereoselective addition of phenylmagnesium bromide to sulfinylimines **6c–e** followed by sequential cleavage of the *O*-silyl and *N*-sulfinyl groups provided optically pure **2c–e**.[40] Both enantiomeric forms were obtained starting from either enantiomer of the Ellman auxiliary. The configuration of compound **8d** was unambiguously established by single crystal X-ray diffraction (Fig. S1), corroborating the previously assigned configuration based on the induction model developed by Ellman.[40,41]

The key step of the cavitand synthesis is the coupling reaction of the enantiopure amines with a suitable calix[5]arene pentacarboxylic acid precursor (**11**, Scheme 2). The use of a temporary protection scheme for the phenol groups was found necessary to improve the efficiency of the coupling reaction and to facilitate purification. Importantly, a small protecting group is required to provide a conformationally flexible calix[5]arene precursor that does not get conformationally locked upon successive condensation reactions (see SI).[42] Herein, we used an allyl protecting group instead of the acetyl group featured in our previous work.[31] The allyl group proved superior due to its greater stability and ease of cleavage under mild conditions under Pd(0)-catalysis. Thus, known pentaaldehyde intermediate **9** was per-alkylated with allyl bromide and subjected to Pinnick oxidation to yield key pentaacid **11** (Scheme 2). Subsequent amide bond formation with chiral amines **2a–e** using standard peptide coupling reagents provided cavitands **12a–e** in good yields, considering the 5-fold reaction. The structure of *O*-allyl derivative (S^5)-**12d** could be determined by single crystal X-ray diffraction (Fig. S3). A molecule of solvent (toluene) was found to be bound in the cavity, demonstrating the capacity of this scaffold to adapt to the bound guest's size and shape while preserving most of the envisaged hydrogen bonding interactions. Finally, cleavage of the allyl groups under Pd(0) catalysis or base induced isomerization conditions (for **12b**) furnished enantiopure cavitands **1a–e** in good overall yields. The structure of (R^5)-**1a** in the solid state could be determined by single crystal X-ray diffraction (Fig. S4). Two solvent molecules are accommodated in the cavity, showcasing the expansion of the binding site upon cleavage of the allyl groups. Overall, we efficiently obtained both enantiomers of 5 different cavitands in enantiopure form through a concise number of steps. The results highlight the potential of this approach to obtain chiral receptors where the electronic properties and molecular recognition abilities can be easily modulated. All hosts were fully characterized by $^1H/^{13}C$ NMR spectroscopy, HRMS, IR spectroscopy, and polarimetry.

The ^1H NMR spectra of cavitands **1a–e** in non-hydrogen bonding solvents such as $CDCl_3$ and toluene-d_8 presented the characteristic features previously observed in lower rim *O*-methyl analogues,[32] namely: (a) separate resonances for the aromatic protons of the calix[5]arene core and the two protons of the methylene bridges, indicating restricted rotation about both the aryl-CH_2 and the aryl-CONH bonds, and (b) far down-

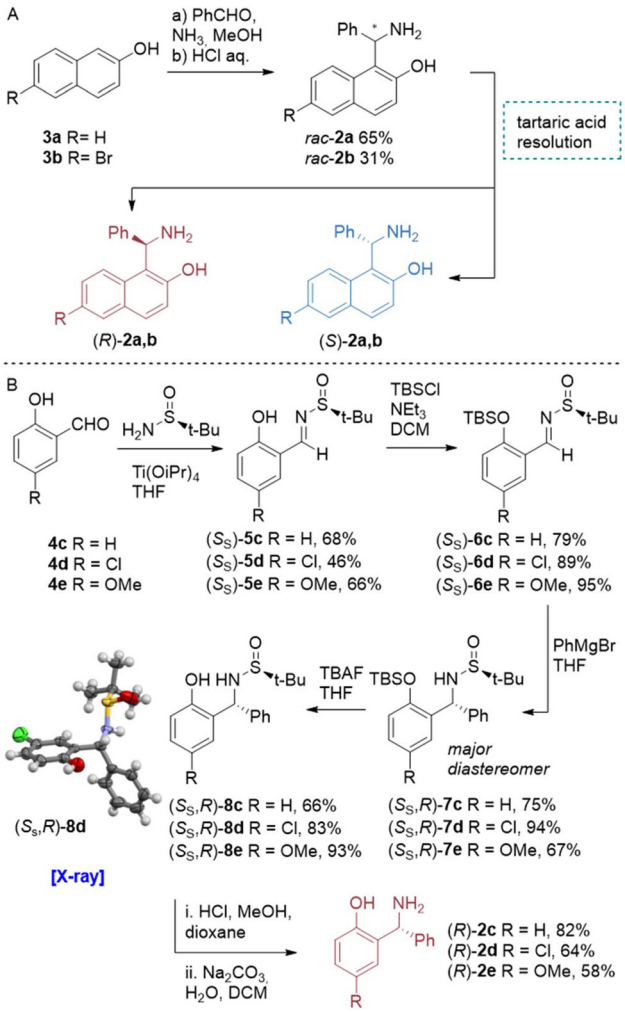

Scheme 1 Synthetic route for the preparation of chiral amine building blocks **2a–e**. A: Naphthol derivatives obtained through conventional resolution. B: Phenol derivatives synthesized *via* a chiral auxiliary strategy. Synthesis of the (*S*)-**2c–e** isomers was conducted analogously starting from (*R*)-2-methylpropane-2-sulfinamide. THF: tetrahydrofuran. TBSCl: *tert*-butyldimethylsilyl chloride. DCM: dichloromethane. TBAF: tetrabutylammonium fluoride.

field shifts corresponding to the OH and NH protons in the upper section of the host, indicative of a cyclic, uninterrupted intramolecular network of cooperative hydrogen bonds (Fig. 2 and Fig. S5). Overall, these features indicate the stabilization through hydrogen bonding of cone conformations that are kinetically stable in the ^{1}H NMR shift time scale.

Fullerene binding

With cavitands **1a–e** in hand, their binding ability toward C_{60}, C_{70}, and PCBM ([6,6]-phenyl-C_{61}-butyric acid methyl ester) was evaluated. We first monitored changes in the ^{1}H NMR spectra of **1a–e** upon addition of fullerenes. As shown in Fig. 2, addition of C_{60} to a solution of **1a** in toluene-d_8 results in the formation of a new set of separate resonances, corroborating the binding event and indicating that the corresponding equilibrium is also slow relative to the ^{1}H NMR time scale. The same behaviour is observed for all the possible cavitand/fullerene combinations. This finding contrasts with the behaviour previously found in lower rim *O*-methyl analogues, which undergo fast guest exchange.[32] Upon binding, all resonances of the cavitand shift downfield, which is commensurate with anisotropic deshielding by the nearby π surface of the fullerene guest. However, the NH and OH resonances experience unusually large downfield shifts, in particular those of the lower rim OH groups, which we attribute to a conformational rigidification of the assembly upon binding of the fullerene guest (Fig. S6 and S7). In order to gauge the substituent effects on the guest exchange kinetics, we systematically determined the barrier of guest exchange using EXSY experiments on solutions of cavitands **1a–e** and PCBM, containing roughly equimolar concentrations of free and bound cavitand (Fig. S8–S12). Interestingly, all the barriers to guest release were found fall in a narrow range ($\Delta G^{\ddagger}$ = 17.1–17.6 kcal mol^{-1}) and no clear correlations to the electronic properties of the phenol/naphthol moiety of the upper panels could be established. This evidence suggests that the cooperativity of the hydrogen bond network is the key feature governing the conformational and guest exchange mechanisms, and that discrete effects that may increase or decrease the hydrogen bonding capability of the OH groups have a negligible effect.

We next determined the association constants (K_a) for the host–guest complexation equilibria of **1a–e** with C_{60}, C_{70} and PCBM, which were found to be in the range of 10^2–10^5 M^{-1} (Table 1). Association constants for C_{60} and C_{70} were determined using UV-vis titrations (Fig. S13 and S14). For PCBM, reliable binding data could not be obtained by UV-Vis titrations. Instead, direct integration of ^{1}H NMR spectra was used to determine K_a, taking advantage of the slow exchange regime as previously detailed (Fig. S15–S19). Additionally, we were able to obtain the thermodynamic parameters of binding for the strongest host–guest pair (C_{70}⊂**1e**) using isothermal titration calorimetry (ITC, Fig. S20). The binding of C_{70} with **1e** is enthalpically favoured and entropically disfavoured (ΔH = −15.2 kcal mol^{-1}; $-T\Delta S$ = 7.5 kcal mol^{-1}). The driving force for binding in the systems studied herein can be dissected in various contributions. First, attractive non-covalent π–π interactions provide an enthalpic gain. The strength of these interactions can be modulated by both the extension of the π system (naphthyl *vs.* phenyl panel) and the electronic effects induced by the panel substituents. Entropic contributions can in turn be broken down in various components. First, desolvation of the fullerenes upon binding has been postulated to be a positive contributor to binding of fullerenes within calixarene hosts.[37] In contrast, the binding event will be accompanied by a conformational selection process of the flexible cavitand structure, as well as a reduction in rotational diffusion of the fullerene, both disfavouring binding in terms of entropy. The entropic penalty to binding determined for C_{70}⊂**1e** is below the intrinsic entropy loss for the formation of a 1 : 1 complex, suggesting that favourable desolvation effects are indeed significant in this system. Some of these contri-

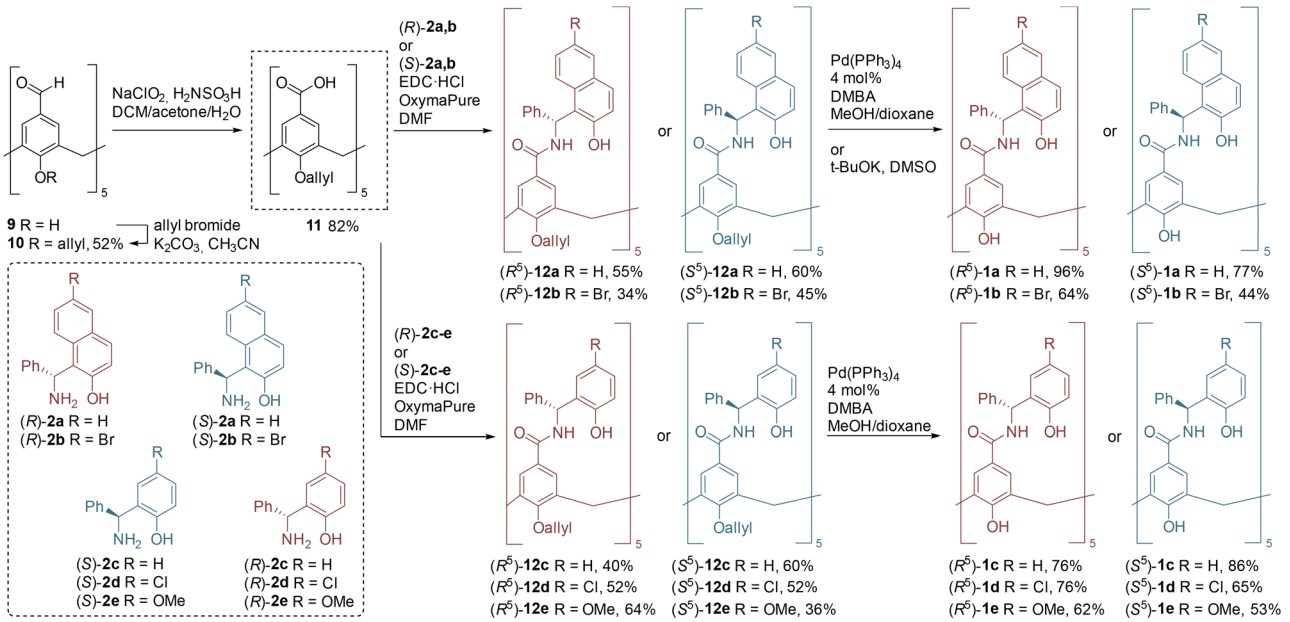

Scheme 2 Synthesis of cavitands **1a–e**. DCM: dichloromethane. OxymaPure: ethyl cyano(hydroxyimino)acetate. EDC·HCl: *N*-(3-dimethylaminopropyl)-*N*′-ethylcarbodiimide hydrochloride. DMF: *N*,*N*-dimethylformamide. DMBA: *N*,*N*′-dimethylbarbituric acid.

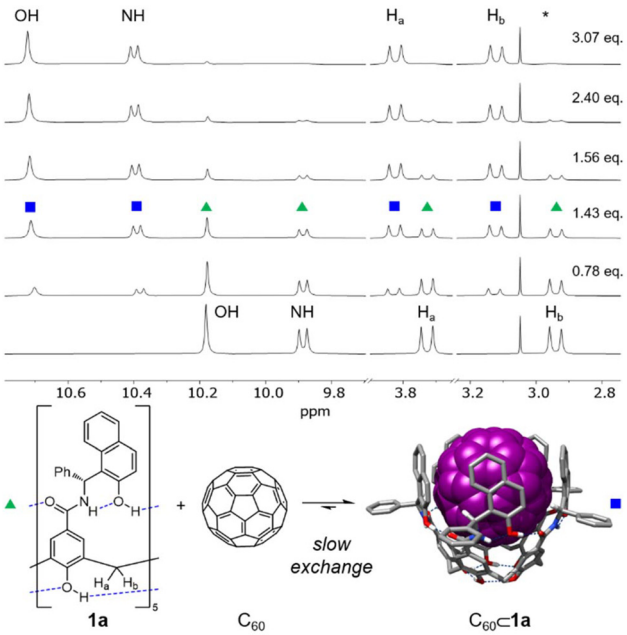

Fig. 2 ^{1}H NMR titration of **1a** with C_{60} (toluene-d_8, [**1a**] = 2.05 mM, 298 K) from bottom spectrum (free **1a**) to top (3.07 eq. C_{60}). The NH/OH and CH_2 regions are shown, highlighting the cooperative nature of the H-bond network and the diastereotopic methylene resonances. Green triangles and blue squares correspond to resonances of free and bound **1a**, respectively. The asterisk indicates residual traces of methanol.

butions to binding may even work in opposite directions. For instance, the extended π surface of naphthyl panels would provide an enhanced enthalpic gain in comparison to phenyl panels, but the latter are less conformationally restricted, which could provide a better overlap with the bound fullerene surface. Overall, the obtained data indicate a complex relationship between cavitand structure and K_a values that points at a delicate balance of factors, although some trends can be obtained. For the naphthalene based cavitands (**1a–b**), the electronic effect is consistent: cavitand **1b** bearing the electron-withdrawing bromine substituents provides lower binding constants throughout the series of fullerenes, which feature a polarizable electron-accepting surface. On the contrary, a consistent electronic effect is not observed for the phenyl panel series (**1c–e**). For C_{60}, introduction of an electron-withdrawing chlorine substituent on the cavitand panels reduces binding while an electron donating methoxy group increases it, as expected (Table 1, entries 3–5), while both chlorine and methoxy groups increase binding in the case of C_{70} and PCBM (Table 1, entries 8–10 and 13–15). In any case **1e**, provides increased binding over **1d** in all cases as expected from electronic effects only. We reason that the phenyl panels provide reduced non-covalent interactions to the bound fullerene with respect to the larger naphthalene π surface, making subtler conformational effects dominant in these cases. Similarly, a clear binding trend when comparing C_{60} and C_{70} is not observed. C_{70} provides the higher K_a in the series (Table 1, entry 10), in good agreement with its poorer solubility in toluene. However, cavitands **1b** and **1c** display increased binding for C_{60}, pointing again at subtle conformational effects. As expected form our previous work,[32,33] the flexibility of the cavitands studied herein allows adaptation to different guest sizes, surpassing the guest complementarity limitations of rigid hosts. Finally, PCBM consistently displayed the lowest affinities throughout the series. While this may be due in part to electronic effects—the π system of C_{60} is partially

Table 1 Association constants (K_a) of cavitands **1a–e** with fullerenes

Cavitand	Entry	Fullerene	K_a [a] [M^{-1}]	Entry	Fullerene	K_a [a] [M^{-1}]	Entry	Fullerene	K_a [b] [M^{-1}]
1a	1	C_{60}	$8.8 \pm 0.4 \times 10^3$	6	C_{70}	$1.6 \pm 0.1 \times 10^4$	11	PCBM	$4.7 \pm 0.2 \times 10^2$
1b	2	C_{60}	$3.8 \pm 0.1 \times 10^2$	7	C_{70}	$1.8 \pm 0.1 \times 10^2$	12	PCBM	$1.8 \pm 0.1 \times 10^2$
1c	3	C_{60}	$1.4 \pm 0.1 \times 10^4$	8	C_{70}	$8.6 \pm 0.3 \times 10^3$	13	PCBM	$4.5 \pm 0.3 \times 10^2$
1d	4	C_{60}	$4.9 \pm 0.3 \times 10^3$	9	C_{70}	$1.7 \pm 0.1 \times 10^4$	14	PCBM	$1.0 \pm 0.1 \times 10^3$
1e	5	C_{60}	$1.4 \pm 0.1 \times 10^4$	10	C_{70}	$1.9 \pm 0.1 \times 10^5$	15	PCBM	$2.7 \pm 0.2 \times 10^3$

[a] Obtained by UV-Vis titration experiments in toluene at 298 K; values are the average of three replicates. [b] Obtained by direct integration from ^{1}H NMR spectra in toluene-d_8, 298 K.

disrupted—entropic effects are likely as important. In comparison to C_{60} and C_{70}, PCBM is intrinsically more soluble in toluene and its cyclopropane addend will lead to reduced rotational diffusion within the cavity. Both effects result in unfavourable entropic contributions.

Chirality transfer to fullerenes

To investigate the ability of the chiral cavitands to induce asymmetry in the fullerene guests, electronic circular dichroism (ECD) measurements were performed on host–guest complexes in solution. These experiments were carried out with excess host over the corresponding fullerene, and the concentrations were adjusted according to the calculated association constants (Table 1) to minimize the amount of free fullerene in solution and maximize the ECD response in the region of the spectrum where only the fullerenes absorb (λ > 400 nm). The observed induced circular dichroism (ICD) signals, quantified by the absorbance dissymmetry factor ($g_{abs} = \Delta A^{R/L}/A$), provided insight into the extent of supramolecular induction. Fig. 3 displays the ECD spectra obtained for the complexes of C_{60}, C_{70}, and PCBM with the (S^5) enantiomers of hosts **1a–e**, highlighting the effect of cavitand structure on the ICD of a given fullerene chromophore (complete spectroscopic data available in the SI, Fig. S21–S23). Given the fact that cavitands **1a–e** do not absorb in the 400–700 nm region (Fig. S24) and that the achiral fullerene molecules are ECD silent, all signals detected in this spectral range are attributable to the host–guest complex and correspond to electronic transitions of the fullerene chromophore. These findings offer clear evidence of chirality transfer from the chiral host to the various fullerene guests. Among all systems examined, the complex PCBM⊂**1e** produced the strongest ICD signals, displaying a maximum g_{abs} of 8.12×10^{-4} (λ = 515 nm). We rationalized this result on the basis of the reduced symmetry of PCBM in relation to C_{60} and C_{70}. In addition, the alkylidene addend on PCBM limits its rotational mobility within the cavity, maximizing the sym-

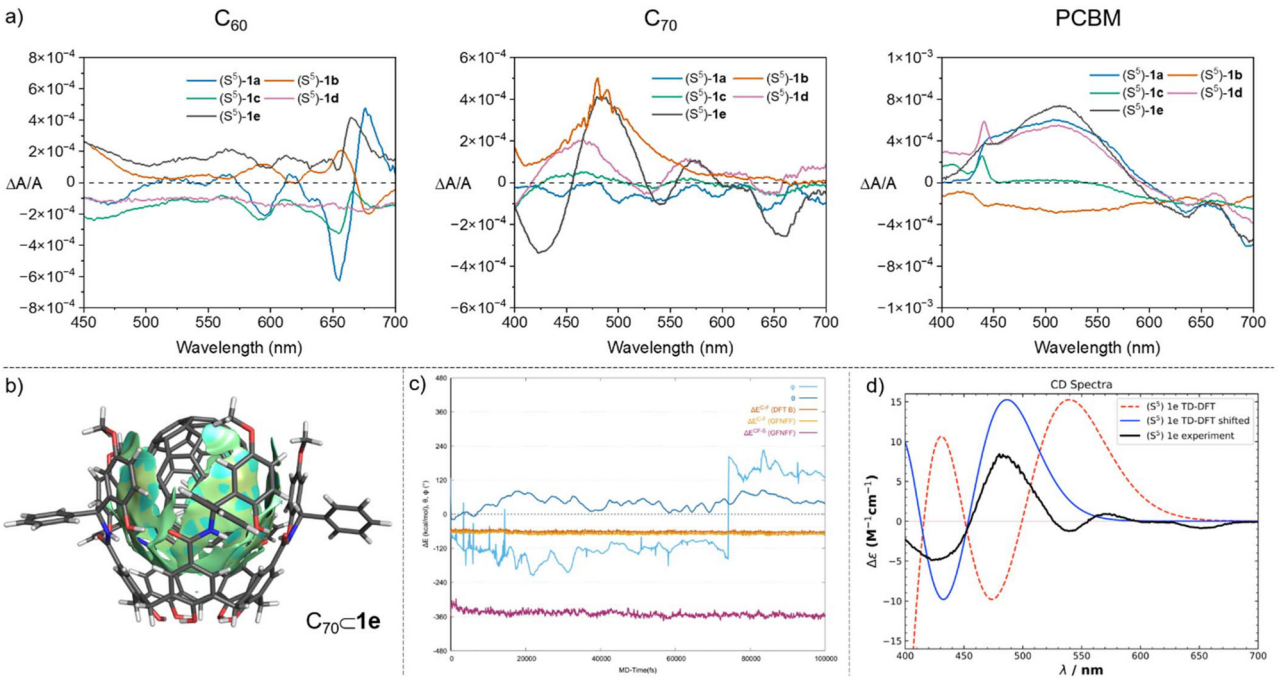

Fig. 3 (a) ECD spectra of C_{60}, C_{70} and PCBM host–guest complexes with **1a–e** in toluene ([**1a–e**] = 10^{-3} M, [fullerene] = 10^{-4} M). (b) NCI plot for C_{70}⊂**1e**. (c) Trajectory analysis for the MD simulation of C_{70}⊂**1e**. (d) Experimental *vs.* computed (TD-DFT, B3LYP/def2-svp) ECD spectra of C_{70}⊂**1e** (see SI for details).

metry breaking of the fullerene chromophore induced by the chiral environment. On the other hand, the lower association constants observed for PCBM ($K_a \sim 10^2$ M^{-1}) indicated a weaker interaction with the aromatic panels that may result in diminished chiral induction. However, cavitands **1a** and **1d** bind C_{70} in the 10^4 M^{-1} range while producing low g_{abs} values ($1.44–2.07 \times 10^{-4}$), indicating that the ICD response is the result of a complex interplay between binding affinity, cavity electronic structure, and guest dynamics. Remarkably, our set of cavitands allows tuning the chiroptical response, producing ECD maxima in a range of frequencies in the visible region, which may be a useful property for building tunable CPL detectors (Fig. 3a). The most salient feature of this cavitand scaffold is the ability to produce varied and complementary chiroptical response with the same fullerene chromophore. This is best illustrated by the pairs of complexes C_{60}⊂**1a**/C_{60}⊂**1b** and PCBM⊂**1a**/PCBM⊂**1b**, where nearly mirror image Cotton effects are obtained from cavitands of the same configuration, by tuning the cavitand–fullerene interactions that lead to chirality transfer through substituent electronic effects only.

Computational studies

Theoretical calculations at different levels were carried out to rationalize the observed molecular recognition phenomena and the resulting chiral induction effects. Structures of all host–guest pairs were optimized by DFT methods, and non-covalent interaction (NCI) analyses were carried out (Fig. 3b and Fig. S25–S27). The results reveal significant favourable host–guest interactions between the surfaces of the fullerene and the aromatic panels of the host, in good agreement with the experimentally obtained binding enthalpy for C_{70}⊂**1e**. Frontier orbital analysis of the host guest complexes revealed that the LUMO of the host guest complexes is located exclusively on the fullerene guest (Fig. S34). On the other hand, the HOMO is distributed across the cavitand surface and the bound fullerene, resulting in breaking of the native fullerene orbital symmetry. The observed induced ECD signals correspond to the HOMO–LUMO transition, an optically forbidden transition, hence the moderate ECD signals observed. Given the innate conformational flexibility of hosts **1a–e** and the potential rotational diffusion of the encapsulated fullerene guests, we carried out molecular dynamics (MD) simulations to rationalize these dynamic effects. The MD trajectories confirmed the flexibility of the receptor scaffold and revealed different degrees of motion among the fullerene guests (Fig. 3c and Fig. S31). The arrangement of PCBM with the cyclopropane addend locked between adjacent panels of the cavitands appears to be significantly stable throughout the trajectories (Fig. S31), which explains the larger g_{abs} values observed for this guest complexes in comparison to cases where the fullerene guest suffers from higher rotational mobility (C_{60}, C_{70}). Finally, the ECD spectra for the complexes of **1e** (the cavitand exhibiting the strongest and most meaningful induced signal across all the range of guests) were simulated using TD-DFT (Fig. 3d and Fig. S33). These simulations reproduced the experimentally observed ECD signals.

Conclusions

We have obtained a new family of self-folding cavitand receptors based on calix[5]arene that allows efficient chirality transfer to bound fullerene guests. A streamlined and highly modular cavitand synthesis has been developed that allows the preparation of cavitands with varied molecular recognition properties. Remarkably, easy access to both enantiomers of these hosts is straightforward and does not require HPLC separation. Despite the cavitands' inherent flexibility, a variety of fullerenes are efficiently bound. Upon binding of fullerenes, an induced ECD signal is obtained in the spectral region of the achiral fullerene guests, showcasing an efficient transfer of chirality in the confined space. This induced chiroptical response can be modulated across the visible region through substituent effects on the cavitand's walls. Overall, this work presents a promising approach for obtaining tailored chiroptical materials based on simple and readily accessible achiral chromophores. Such materials could find applications in the development of CPL sensors[29] or quantum information technologies based on the CISS effect of discrete molecular entities.[43]

Author contributions

H. M. L. carried out the synthesis of cavitands, acquired spectroscopic and titration data, analysed and curated the data, and edited the manuscript. A. S. B and F. F. carried out computational work and curated the corresponding data. C. M.-A. and P G.-M. synthesized intermediates of cavitands **1a–e**. E. P.-F. acquired and curated ECD spectroscopic data. M. S. planned and supervised computational work, analysed the data, edited the manuscript, and was responsible for funding acquisition. A. L. conceptualized the project, designed experiments, analysed and curated the data, wrote the manuscript and was responsible for funding acquisition.

Conflicts of interest

There are no conflicts to declare.

Data availability

The data supporting the findings of this work has been deposited in the CORA. RDR repository,[44] **https://doi.org/10.34810/data2722**.

Supplementary information (SI): synthesis procedures, characterization data, titration data, computational details. See DOI: **https://doi.org/10.1039/d6qo00249h**.

CCDC 2527221 (**8d**), 2527222 (**9**), 2533645 ((*S*^{5})-**12d**) and 2548699 ((*R*^{5})-**1a**) contain the supplementary crystallographic data for this paper.[45a–d]

Acknowledgements

We are grateful for financial support from grants TED2021-130573B-I00, PID2023-146498NB-I00, PID2023-152415NB-I00, RED2024-154A8-T, REQ2021_B_05, and fellowship PREP2023-002111 (to F. F.) funded by MICIU/AEI/10.13039/501100011033 and by the European Union NextGenerationEU/PRTR. We thank AGAUR/Generalitat de Catalunya for funding (2021SGR623 and 2021SGR00487) and the Universitat de Girona for a fellowship to A. S. B. (IFUdG 68 2022). E. P. thanks ICIQ for a predoctoral contract. We thank Dr Xavier Fontrodona (Serveis Tècnics de Recerca, Universitat de Girona) for solving X-ray diffraction structures.

References

1 J. Liu, L. Qiu and S. Shao, Emerging electronic applications of fullerene derivatives: an era beyond OPV, *J. Mater. Chem. C*, 2021, **9**, 16143–16163.
2 A. Montellano López, A. Mateo-Alonso and M. Prato, Materials chemistry of fullerene C60 derivatives, *J. Mater. Chem.*, 2011, **21**, 1305–1318.
3 E. Castro, A. H. Garcia, G. Zavala and L. Echegoyen, Fullerenes in biology and medicine, *J. Mater. Chem. B*, 2017, **5**, 6523–6535.
4 X. Chang, Y. Xu and M. von Delius, Recent advances in supramolecular fullerene chemistry, *Chem. Soc. Rev.*, 2024, **53**, 47–83.
5 S. Mirzaei, H. Khosravi, X. Hu, M. S. Mirzaei, V. M. E. Castro, X. Wang, N. A. Figueroa, T. Chang, Y.-P. Chen, G. P. Ríos, N. I. Gonzalez-Pech, Y.-S. Chen and R. Hernández Sánchez, Catching Fullerenes: Synthesis of Molecular Nanogloves, *Angew. Chem., Int. Ed.*, 2025, e202505083.
6 J. Pfeuffer-Rooschüz, S. Heim, A. Prescimone and K. Tiefenbacher, Megalo-Cavitands: Synthesis of Acridane [4]arenes and Formation of Large, Deep Cavitands for Selective C70 Uptake, *Angew. Chem., Int. Ed.*, 2022, **61**, e202209885.
7 C. Fuertes-Espinosa, J. Murillo, M. E. Soto, M. R. Ceron, R. Morales-Martínez, A. Rodríguez-Fortea, J. M. Poblet, L. Echegoyen and X. Ribas, Highly selective encapsulation and purification of U-based C78-EMFs within a supramolecular nanocapsule, *Nanoscale*, 2019, **11**, 23035–23041.
8 Y. Shi, K. Cai, H. Xiao, Z. Liu, J. Zhou, D. Shen, Y. Qiu, Q.-H. Guo, C. Stern, M. R. Wasielewski, F. Diederich, W. A. Goddard III and J. F. Stoddart, Selective Extraction of C70 by a Tetragonal Prismatic Porphyrin Cage, *J. Am. Chem. Soc.*, 2018, **140**, 13835–13842.
9 S.-i. Kawano, T. Fukushima and K. Tanaka, Specific and Oriented Encapsulation of Fullerene C70 into a Supramolecular Double-Decker Cage Composed of Shape-Persistent Macrocycles, *Angew. Chem., Int. Ed.*, 2018, **57**, 14827–14831.
10 C. Fuertes-Espinosa, A. Gómez-Torres, R. Morales-Martínez, A. Rodríguez-Fortea, C. García-Simón, F. Gándara, I. Imaz, J. Juanhuix, D. Maspoch, J. M. Poblet, L. Echegoyen and X. Ribas, Purification of Uranium-based Endohedral Metallofullerenes (EMFs) by Selective Supramolecular Encapsulation and Release, *Angew. Chem., Int. Ed.*, 2018, **57**, 11294–11299.
11 G. Markiewicz, A. Jenczak, M. Kołodziejski, J. J. Holstein, J. K. M. Sanders and A. R. Stefankiewicz, Selective C70 encapsulation by a robust octameric nanospheroid held together by 48 cooperative hydrogen bonds, *Nat. Commun.*, 2017, **8**, 15109.
12 C. Fuertes-Espinosa, C. García-Simón, E. Castro, M. Costas, L. Echegoyen and X. Ribas, A Copper-based Supramolecular Nanocapsule that Enables Straightforward Purification of Sc3N-based Endohedral Metallofullerene Soots, *Chem. – Eur. J.*, 2017, **23**, 3553–3557.
13 C. García-Simón, M. Garcia-Borràs, L. Gómez, T. Parella, S. Osuna, J. Juanhuix, I. Imaz, D. Maspoch, M. Costas and X. Ribas, Sponge-like molecular cage for purification of fullerenes, *Nat. Commun.*, 2014, **5**, 5557.
14 T. Pèlachs, C. Sabrià, V. Iannace, I. Imaz, F. Gándara, D. Maspoch, F. Feixas and X. Ribas, Supramolecular Mask Regioconverter: Orthogonal Diels–Alder C70 Bisadducts by Mask-Mediated Regioselective Synthesis, *CCS Chemistry*, 2024, **7**, 703–715.
15 V. Iannace, C. Sabrià, Y. Xu, M. v. Delius, I. Imaz, D. Maspoch, F. Feixas and X. Ribas, Regioswitchable Bingel Bis-Functionalization of Fullerene C70 via Supramolecular Masks, *J. Am. Chem. Soc.*, 2024, **146**, 5186–5194.
16 Z. Lu, T. K. Ronson, A. W. Heard, S. Feldmann, N. Vanthuyne, A. Martinez and J. R. Nitschke, Enantioselective fullerene functionalization through stereochemical information transfer from a self-assembled cage, *Nat. Chem.*, 2023, **15**, 405–412.
17 E. Ubasart, O. Borodin, C. Fuertes-Espinosa, Y. Xu, C. García-Simón, L. Gómez, J. Juanhuix, F. Gándara, I. Imaz, D. Maspoch, M. von Delius and X. Ribas, A three-shell supramolecular complex enables the symmetry-mismatched chemo- and regioselective bis-functionalization of C60, *Nat. Chem.*, 2021, **13**, 420–427.
18 V. Leonhardt, S. Fimmel, A.-M. Krause and F. Beuerle, A covalent organic cage compound acting as a supramolecular shadow mask for the regioselective functionalization of C60, *Chem. Sci.*, 2020, **11**, 8409–8415.
19 C. Fuertes-Espinosa, M. Pujals and X. Ribas, Supramolecular Purification and Regioselective Functionalization of Fullerenes and Endohedral Metallofullerenes, *Chem*, 2020, **6**, 3219–3262.
20 C. Fuertes-Espinosa, C. García-Simón, M. Pujals, M. Garcia-Borràs, L. Gómez, T. Parella, J. Juanhuix, I. Imaz,

D. Maspoch, M. Costas and X. Ribas, Supramolecular Fullerene Sponges as Catalytic Masks for Regioselective Functionalization of C60, *Chem*, 2020, **6**, 169–186.

21 H. Sasafuchi, M. Ueda, N. Kishida, T. Sawada, S. Suzuki, Y. Imai and M. Yoshizawa, Remote optical chirality transfer via helical polyaromatic capsules upon encapsulation, *Chem*, 2025, **11**, 102332.

22 E. Benchimol, H. M. O'Connor, B. Schmidt, N. Bogo, J. J. Holstein, J. I. Lovitt, S. Shanmugaraju, C. J. Stein, T. Gunnlaugsson and G. H. Clever, Chiral Pd2L4 Capsules from Readily Accessible Tröger's Base Ligands Inducing Circular Dichroism on Fullerenes C60 and C70, *Angew. Chem., Int. Ed.*, 2024, e202421137.

23 J. Kou, Q. Wu, D. Cui, Y. Geng, K. Zhang, M. Zhang, H. Zang, X. Wang, Z. Su and C. Sun, Selective Encapsulation and Chiral Induction of C60 and C70 Fullerenes by Axially Chiral Porous Aromatic Cages, *Angew. Chem., Int. Ed.*, 2023, **62**, e202312733.

24 M. Yamamura, T. Saito, T. Hasegawa, E. Nishibori and T. Nabeshima, Synthesis of a chiral metallo-capsule composed of concave molecules and chirogenesis upon fullerene binding, *Chem. Commun.*, 2021, **57**, 8754–8757.

25 G. D. Pantoş, J.-L. Wietor and J. K. M. Sanders, Filling Helical Nanotubes with C60, *Angew. Chem., Int. Ed.*, 2007, **46**, 2238–2240.

26 Z.-i. Yoshida, H. Takekuma, S.-i. Takekuma and Y. Matsubara, Molecular Recognition of C60 with γ-Cyclodextrin, *Angew. Chem., Int. Ed. Engl.*, 1994, **33**, 1597–1599.

27 T. Liu, I. Abrahams and T. J. S. Dennis, Structural Identification of 19 Purified Isomers of the OPV Acceptor Material bisPCBM by ^{13}C NMR and UV–Vis Absorption Spectroscopy and High-Performance Liquid Chromatography, *J. Phys. Chem. A*, 2018, **122**, 4138–4152.

28 M. Lenes, G.-J. A. H. Wetzelaer, F. B. Kooistra, S. C. Veenstra, J. C. Hummelen and P. W. M. Blom, Fullerene Bisadducts for Enhanced Open-Circuit Voltages and Efficiencies in Polymer Solar Cells, *Adv. Mater.*, 2008, **20**, 2116–2119.

29 W. Shi, F. Salerno, M. D. Ward, A. Santana-Bonilla, J. Wade, X. Hou, T. Liu, T. J. S. Dennis, A. J. Campbell, K. E. Jelfs and M. J. Fuchter, Fullerene Desymmetrization as a Means to Achieve Single-Enantiomer Electron Acceptors with Maximized Chiroptical Responsiveness, *Adv. Mater.*, 2021, **33**, 2004115.

30 R. Álvarez-Yebra, R. López-Coll, N. Clos-Garrido, D. Lozano and A. Lledó, Calix[5]arene Self-Folding Cavitands: A New Family of Bio-Inspired Receptors with Enhanced Induced Fit Behavior, *Isr. J. Chem.*, 2024, **64**, e202300077.

31 R. Álvarez-Yebra, A. Sors-Vendrell and A. Lledó, Intermolecular hydrogen bonding in calix[5]arene derived cavitands regulates the molecular recognition of fullerenes, *Chem. Commun.*, 2023, **59**, 11556–11559.

32 R. Álvarez-Yebra, R. López-Coll, P. Galán-Masferrer and A. Lledó, Enantioselective Molecular Recognition in a Flexible Self-Folding Cavitand, *Org. Lett.*, 2023, **25**, 3190–3194.

33 D. Lozano, R. Álvarez-Yebra, R. López-Coll and A. Lledó, A flexible self-folding receptor for coronene, *Chem. Sci.*, 2019, **10**, 10351–10355.

34 T. Haino, C. Fukunaga and Y. Fukazawa, A New Calix[5]arene-Based Container: Selective Extraction of Higher Fullerenes, *Org. Lett.*, 2006, **8**, 3545–3548.

35 T. Haino, M. Yanase and Y. Fukazawa, Fullerenes Enclosed in Bridged Calix[5]arenes, *Angew. Chem., Int. Ed.*, 1998, **37**, 997–998.

36 T. Haino, M. Yanase and Y. Fukazawa, Crystalline supramolecular complexes of C60 with calix[5]arenes, *Tetrahedron Lett.*, 1997, **38**, 3739–3742.

37 T. Haino, M. Yanase and Y. Fukazawa, New Supramolecular Complex of C60 Based on Calix[5]arene—Its Structure in the Crystal and in Solution, *Angew. Chem., Int. Ed. Engl.*, 1997, **36**, 259–260.

38 Y. Dong, R. Li, J. Lu, X. Xu, X. Wang and Y. Hu, An Efficient Kinetic Resolution of Racemic Betti Base Based on an Enantioselective N,O-Deketalization, *J. Org. Chem.*, 2005, **70**, 8617–8620.

39 M. Betti, β-Naphthol phenylaminomethane, *Org. Synth.*, 1929, **9**, 60.

40 A. Quintavalla, R. Veronesi, D. Zambardino, D. Carboni and M. Lombardo, Diastereoselective Synthesis of Chiral Oxathiazine 2-Oxide Scaffolds as Sulfinyl Transfer Agents, *Adv. Synth. Catal.*, 2022, **364**, 1695–1700.

41 M. T. Robak, M. A. Herbage and J. A. Ellman, Synthesis and Applications of tert-Butanesulfinamide, *Chem. Rev.*, 2010, **110**, 3600–3740.

42 D. R. Stewart, M. Krawiec, R. P. Kashyap, W. H. Watson and C. D. Gutsche, Conformational Characteristics of Ethers and Esters of p-tert-Butylcalix[5]arene, *J. Am. Chem. Soc.*, 1995, **117**, 586–601.

43 H. J. Eckvahl, N. A. Tcyrulnikov, A. Chiesa, J. M. Bradley, R. M. Young, S. Carretta, M. D. Krzyaniak and M. R. Wasielewski, Direct observation of chirality-induced spin selectivity in electron donor–acceptor molecules, *Science*, 2023, **382**, 197–201.

44 H. Marchi Luciano, C. Montiel-Andreotti, E. Prat-Font, P. Galán-Masferrer and A. Lledó, *Replication data for A modular family of chiral cavitand receptors: tuning the chiroptical response of achiral fullerene guests*, CORA. Repositori de Dades de Recerca, 2026. DOI: **10.34810/data2722**.

45 (*a*) CCDC 2527221: Experimental Crystal Structure Determination, 2026, DOI: **10.5517/ccdc.csd.cc2qts8m**; (*b*) CCDC 2527222: Experimental Crystal Structure Determination, 2026, DOI: **10.5517/ccdc.csd.cc2qts9n**; (*c*) CCDC 2533645: Experimental Crystal Structure Determination, 2026, DOI: **10.5517/ccdc.csd.cc2r1ghs**; (*d*) CCDC 2548699: Experimental Crystal Structure Determination, 2026, DOI: **10.5517/ccdc.csd.cc2rk43l**.

